Chapter 10

Laser-Induced Plasma and its Applications

Kashif Chaudhary, Syed Zuhaib Haider Rizvi and Jalil Ali

Additional information is available at the end of the chapter

http://dx.doi.org/10.5772/61784

Abstract

The laser irradiation have shown a range of applications from fabricating, melting, and evaporating nanoparticles to changing their shape, structure, size, and size distribution. Laser induced plasma has used for different diagnostic and technological applications as detection, thin film deposition, and elemental identification. The possible interferences of atomic or molecular species are used to specify organic, inorganic or biological materials which allows critical applications in defense (landmines, explosive, forensic (trace of explosive or organic materials), public health (toxic substances pharmaceutical products), or environment (organic wastes). Laser induced plasma for organic material potentially provide fast sensor systems for explosive trace and pathogen biological agent detection and analysis. The laser ablation process starts with electronic energy absorption (~fs) and ends at particle recondensation (~ms). Then, the ablation process can be governed by thermal, non-thermal processes or a combination of both. There are several types of models, i.e., thermal, mechanical, photophysical, photochemical and defect models, which describe the ablation process by one dominant mechanism only. Plasma ignition process includes bond breaking and plasma shielding during the laser pulse. Bond breaking mechanisms influence the quantity and form of energy (kinetic, ionization and excitation) that atoms and ions can acquire. Plasma expansion depends on the initial mass and energy in the plume. The process is governed by initial plasma properties (electron density, temperature, velocity) after the laser pulse and the expansion medium. During first microsecond after the laser pulse, plume expansion is adiabatic afterwards line radiation becomes the dominant mechanism of energy loss.

Keywords: Laser Induced Plasma, Plasma Diagnostics, Plasma Applications

1. Introduction

Laser-induced plasma (LIP) formation is a rapid process that is under investigation for several decades due to its versatile and complex nature. Intense laser pulse delivers energy to the target surface for a very short interval of time that instantly excites, ionizes and vaporizes the material

into an extremely hot vapour plume also called as 'plasma plume'. It has three main regions as depicted in Figure 1. Near the target surface is the hottest and the densest part of the plasma called core; in this region, the material is mostly found in the ionized state because of high temperatures. Within the core adjacent to the target surface there exists a so-called *Knudsen layer* having a thickness equal to a few mean free paths. *Knudsen layer* is defined as the region in which a particle achieves an equilibrium velocity distribution from non-equilibrium distribution within a few mean-free paths [1]. In the mid-region of plasma, ions and neutrals (atoms + molecules) coexist due to the ongoing ionization and recombination processes. The outermost region of the plasma is relatively cold, where the population of neutrals dominates and may absorb the radiations coming out of the core and mid-regions of the plasma. Beyond it, there is a shock wave front produced due to the explosive expansion of the plasma, and travels ahead of the plasma plume.

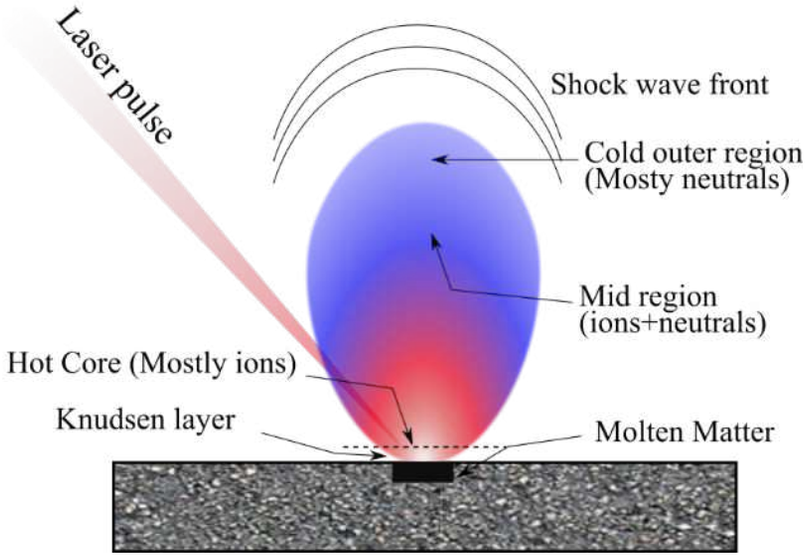

Figure 1. Schematic illustration of laser-induced plasma

In this chapter, the interaction of short (~nanosecond (ns)) and ultrashort (~picosecond (ps) and femtosecond (fs)) laser pulses with a variety of media, pulsed laser ablation (PLA), laser-induced plasma, plasma diagnostic techniques and applications of LIP is discussed. Out of the large canvas, the description about standard plasma diagnostic techniques encompassing optical emission spectroscopy (OES), laser-induced fluorescence (LIF), Langmuir probe, Faraday's cups and solid-state nuclear track detectors (SSNTDs) is provided. As the last section of the chapter, extensive literature review is presented that elaborates applications of the laser-induced plasma. Applications of laser-induced plasma in two main fields, that is, laser-induced breakdown spectroscopy (LIBS) and thin-film or pulsed laser deposition (PLD), are discussed in diverse fields of science and technology.

http://dx.doi.org/10.5772/61784

2. Laser–matter interaction

Lasers are unique energy sources characterized by their spectral purity, spatial and temporal coherence and high intensity. When laser interacts with matter, it can reflect, scatter, absorb or transmit depending upon the material characteristics (i.e. composition, physical, chemical and optical properties) and laser parameters. Laser energy, wavelength, spatial and temporal coherence, exposure time/pulse duration, etc. are the key influential parameters in laser–matter interaction.

The laser basically interacts with electrons in the material by energy transfer and excitation. Free electrons absorb energy and accelerate, whereas bound electrons excite to higher energy levels if laser photons match the bandgap energy of atoms. This absorbed energy is later released by the excited/accelerated electrons as electromagnetic radiation or dissipate into lattice as heat energy.

Different types of interactions of laser with the matter have found various applications. However, this chapter focuses on the laser-induced plasma that is, primarily, the consequence of laser energy absorption in the material. The interaction of laser is different for different materials.

In *metals*, there are a large number of free electrons available; the laser energy excites these electrons to various energies. The excitation of free electrons is taken as the increase in their kinetic energy. As free electrons are excited, the collision rate increases and the energy is transferred from the excited free electrons to lattice phonons.

Since *semiconductors* and *insulators* have very few free electrons, the laser interacts with bound electrons in atomic/ionic shells and generates electron–hole pairs. The generation of electron–hole pair depends upon the laser photon energy. If it matches the material's bandgap 'E_g', that is, the energy difference between the highest level in valence band and lowest level in the conduction band, an electron–hole pair is generated. If it is lower than the E_g, the photon may not absorb or cause low-energy intra-band electronic excitations in vibrational states.

In *dielectrics*, the laser energy causes ionization and liberates electrons within the material. Once the free electrons are available, collisional ionization starts that is termed as impact or avalanche ionization. It forms a dense cloud of ions near the surface that is opaque to the laser and absorbs later part of the laser pulse. In dense *ceramics*, the laser interaction phenomenon is same as in dielectrics; however, in the porous *ceramics*, the laser is mostly scattered due to the random distribution of particle size.

3. Pulsed laser ablation

Pulsed laser ablation is a high-photon-yield sputtering phenomenon in which the material is removed from a solid surface by the interaction of high-intensity short laser pulses. It is consequence of the conversion of laser-induced electronic and vibration excitation into the

kinetic energy of nuclear motion. The material removal rate typically exceeds one-tenth of a monolayer per pulse that alters the surface composition at mesoscale. If particles are ejected out of the surface but there is no detectable modification in the surface composition, it is commonly referred to as *laser-induced desorption*. Being a mesoscale phenomenon, PLA is influenced by bulk properties of the material, for example, elasticity and compressibility. Moreover, the laser ablation need not involve massive, catastrophic destruction of the surface.

In pulsed laser ablation,

- The total yield of ejected particles is strongly proportional to the density of electronic and vibrational excitation.
- There is a threshold for photon fluence, below which only desorption can take place with negligible material damage.

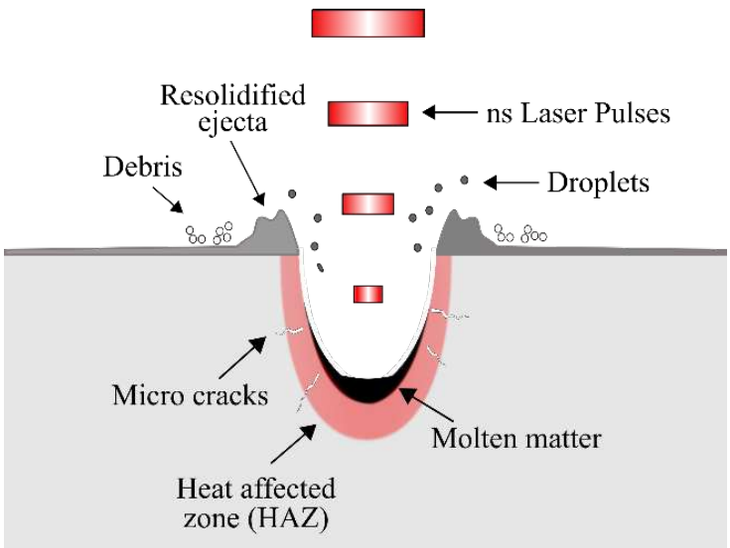

Figure 2. Illustration of nanosecond pulsed-laser ablation

PLA is a useful technique for surface machining. Although microcracks and heat-affected zone (HAZ) are formed as a result of thermal stresses and heat conduction into the bulk medium as illustrated in Figure 2, PLA provides an advantage of minimizing the heat-affected zone under certain circumstances. In the case of nanosecond laser pulses, the heat-affected zone will be minimal if the ablation depth per pulse Δh is comparable to the thermal penetration depth $l_t \approx 2\sqrt{D\tau_l}$ or the optical penetration depth $l_\alpha \approx \alpha^{-1}$ [2]:

$$\Delta h \approx \max\{l_\alpha, l_t\} \tag{1}$$

where D represents thermal diffusivity of the material, τ_l is the laser pulse duration and α is the optical absorption of the material. In case of ablation with ultrashort laser pulses, HAZ is nearly absent or is negligible due to non-thermal mechanisms governing the ablation.

http://dx.doi.org/10.5772/61784

3.1. Mechanisms of laser ablation

Laser ablation mechanisms are different for short (~ns) and ultrashort (~ps and fs) laser pulses due to the difference in laser coupling with matter at different timescales involved. Short pulse, that is, nanosecond pulse ablation, can be characterized through thermal, non-thermal and combination of both mechanisms. These are also referred to as photo-thermal, photo-chemical and photo-physical mechanisms, respectively. However, for certain experimental parameters and materials, the ablation can be described through one dominant mechanism.

If the excited material quickly converts the absorbed laser energy into heat, high temperature can build up near surface stresses in the material, which can lead to material ablation off the surface. Such an ablation is governed by the photo-thermal mechanism.

If the incoming laser photons have sufficiently high energy, the absorption can induce defects in the material or cause direct bond breaking of atoms, ions or molecules. Defects and bond breaking can individually cause ablation of the material. Such an ablation is termed as photo-chemical ablation. However, if the ablation occurs as a result of both thermal and non-thermal mechanisms, it is termed as photo-physical ablation. Figure 3 graphically illustrates the laser ablation process through thermal, non-thermal and photo-physical processes.

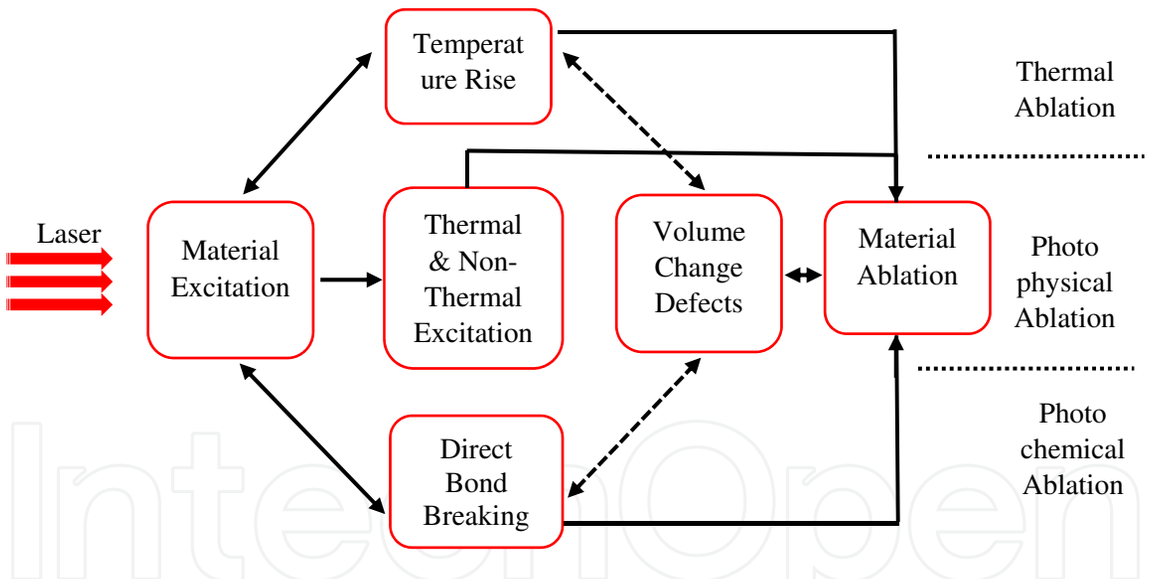

Figure 3. Graphical illustration of mechanisms leading to pulsed laser ablation

In case of ultrashort laser pulses, the mechanisms of photon absorption, heat transfer within the material and hydrodynamic ablation take place at different timescales independent of each other [3]. The phenomena that are not important or less significant in short-pulse laser ablation become dominant and significant because of ultrashort timescales and extreme laser intensities involved. Nonlinear absorption, Coulomb explosion and overcritical heating are the dominant phenomena in ultrashort pulsed laser ablation. At low laser intensities, close to the ablation threshold, Coulomb explosion governs the ablation. The absorbed laser energy accelerates electrons, and if the energy is sufficient to overcome the binding energy and work function of

the material, electrons eject from the surface and form a charged cloud (of electrons) above the material surface leaving behind a charge density of ions on the surface. It creates a space charge separation; the electric field within the charge separation can be so strong that it can pull ions out of the material resulting in removal of top few monolayers from the surface [4]. Because of enormous intensities, non-linear multiphoton absorption phenomenon increases the laser energy absorption in the material that leads to cascade ionization. At ultrashort timescales (~pico- and femtoseconds), the material cannot either transfer energy to the lattice or evaporate instantly, rather the absorbed laser energy causes extreme excitation and heating of the material above critical temperatures. Consequently, a rapidly expanding mixture of liquid droplets and vapours is observed above the target surface [5].

4. Laser-induced plasma formation

4.1. Plasma ignition

Laser ablation can be divided into three phases

- Bond-breaking and plasma ignition
- Plasma expansion and cooling
- Particle ejection and condensation

The laser ablation process starts with electronic energy absorption (~fs) and ends at particle recondensation (~ms). Plasma ignition process includes bond breaking and plasma shielding during the laser pulse interaction with the material surface. Bond-breaking mechanisms influence the quantity and form of energy (kinetic, ionization and excitation) that atoms and ions can acquire.

For nanosecond laser pulses of irradiance < 10^8 W/cm^2, the dominant mechanism of plasma ignition is thermal vaporization [6], whereas for picosecond laser pulses with irradiances between 10^8 and 10^{13} W/cm^2 both thermal and non-thermal mechanisms contribute to the plasma ignition. However, with femtosecond laser pulses of irradiance > 10^{13}W/cm^2, the main bond-breaking (plasma ignition) mechanism is non-thermal, that is, Coulomb's explosion [6].

4.2. Plasma expansion and cooling

Plasma expansion depends on the initial mass and energy in the plume. The process is governed by initial plasma properties (electron density, temperature and velocity) after the laser pulse and the expansion medium. During the first microsecond after the laser pulse, plume expansion is adiabatic; afterwards, line radiation becomes the dominant mechanism of energy loss.

4.3. Particle formation and condensation

Condensation or particle formation takes place during the decay/cooling process of plasma. It starts when plasma temperature reaches the boiling point of the material and stops at the

condensation temperature of the material. Exfoliation can also be observed as a result of high thermal stresses within the material due to fast heating. Thermal stresses produced in the material can break it into irregularly shaped particles that may eject from the surface. This phenomenon is called as exfoliation.

5. Plasma diagnostic techniques

Plasma is a rich source of radiations. A wide spectrum of electromagnetic radiation ranging from IR through X-rays is emitted by excited species of the plasma that is of practical interest. Various specialized techniques are utilized for the diagnostics of specific radiations emitting from the plasma. Diagnostic techniques can largely be categorized in optical diagnostic techniques, electrical diagnostic techniques and diagnostics using solid-state detectors. Optical diagnostics of the plasma gives indirect estimation of plasma conditions based on characteristics of plasma emission spectrum. However, electrical diagnostic techniques provide direct measurements of plasma characteristics and X-rays, electron and ion emissions from the plasma. For energy distribution of particles emitting from plasma, solid-state detectors are brought into use.

5.1. Optical diagnostics

Due to fast process and short lifetime, not all optical diagnostic techniques are useful to study laser-induced plasma that are used for persistent plasmas like inductively coupled plasma (ICP) and plasma focus (PF). The most common technique used for optical diagnostics of laser-induced plasma is emission spectroscopy. Radiations emitted from the plasma are collected by a spectrometer or a monochromator depending on the nature of study. Spectrometer captures a range of electromagnetic spectrum by a charge-coupled device (CCD) detector or with intensified CCD for even better results, whereas in monochromator a specific wavelength or a band is studied in high resolution with a CCD detector of a photomultiplier tube (PMT).

The spectrum is obtained as a combination of characteristic line emissions and continuum emissions. These spectra carry loads of information about the plasma conditions and composition. Various features of the spectrum can be utilized to obtain specific information about the plasma. For example, Doppler broadening of an emission line is related to velocity of the emitting particle, intensity of the emission line is proportional to the quantity of the emitter, Stark broadening of the line tells about electron density in the plasma while the ratio between intensity of emission line and continuum can provide us with temperature of the plasma, etc.

Another optical technique that is used for highly localized study of laser-induced plasma diagnostics is the laser-induced fluorescence. A tunable laser tuned to a specific wavelength, which is passed through the plasma to excite specific elements for certain transitions. In turn, upon de-excitation, radiations of a different frequency are obtained that help in studying the species of interest in the plasma. However, such a system is less popular because of the difficult set-up and expensive equipment. A combined system for plasma diagnostics through optical emission spectroscopy and laser-induced fluorescence is schematically shown in Figure 4.

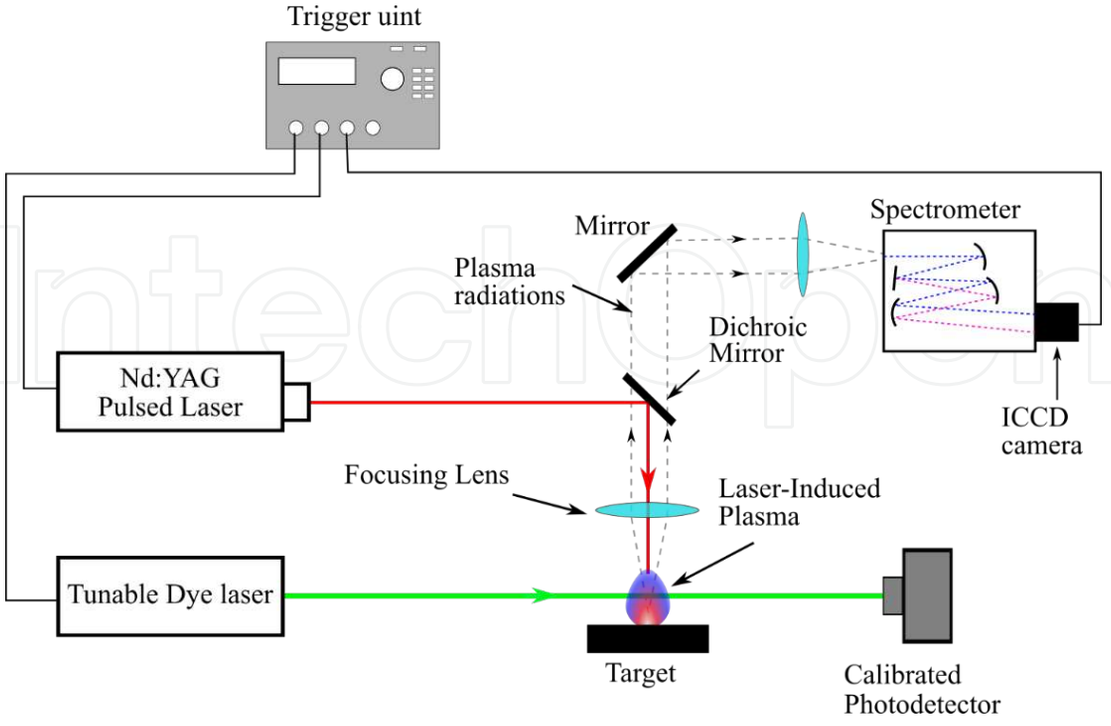

Figure 4. Schematic illustration of a combined set-up of laser-induced fluorescence and optical emission spectroscopy of laser-induced plasma

5.1.1. Electron density measurements

Electron density in the plasma can be measured through Stark broadening of an emission line or through the intensity ratio of two different emission lines of the same element. Utilizing the Stark-broadening method is considered more reliable because broadening of the emission line due to the Stark effect is a direct consequence of the presence of charged particles around the emitter.

For estimation of electron density in the plasma by making use of Stark broadening of an emission line, correct measurement of the Stark broadening is important. The emission line is normally broadened by a combination of three broadening mechanisms, that is, natural broadening, Doppler broadening that is caused by thermal motion of the emitter and Stark broadening caused by splitting of energy level because of the electric field strength of charged particles near the emitter. Doppler broadening is prominent at high temperatures, whereas the Stark broadening, which is also called as collision or pressure broadening, dominates at high densities of charged particles in the plasma.

Natural line broadening is related to naturally existing split in an energy level that makes an energy band. It can be related to the uncertainty in the energy of an excited state 'ΔE' for a limited excitation time 'Δt' of an electron through Heisenberg's uncertainty principle as $\sim \Delta E \Delta t > \hbar$. Normally, natural broadening is so small that it is undetectable by the spectrometers typically used in plasma diagnostics.

Doppler line broadening is a consequence of thermal motion of the emitter along the line of observation. The variation in the wavelength is explained on the basis of the Doppler effect. If movement of the emitter is towards the detector, a slightly shorter wavelength is recorded, and if the movement is away from the detector, a slightly longer wavelength is observed by the detector. Consequently, a broader emission line with a Gaussian profile is observed. For an emitter of atomic mass M, Doppler broadening $\Delta\lambda_D$ of an emission line at wavelength λ for a particular electron temperature T can be calculated as

$$\Delta\lambda_D = 2\lambda\sqrt{\frac{2kT\ln 2}{Mc^2}} \tag{2}$$

In addition to the above-described broadenings, the emission line is superimposed by another broadening contributed by the spectrometer itself that is referred to as *instrumental broadening*. It can be determined by using a narrow line laser beam. Typically, Doppler and Stark are the main competing broadening mechanisms. At high temperatures, Doppler broadening can be dominant, whereas at high densities Stark can be a dominant broadening mechanism. When Doppler broadening is negligible and Stark broadening mechanism is the main broadening mechanism, Stark broadening $\Delta\lambda_{stark}$ can be isolated from the instrumental broadening $\Delta\lambda_{stark}$ by deconvolution:

$$\Delta\lambda_{stark} = \Delta\lambda_{total} - \Delta\lambda_{instumental} \tag{3}$$

Stark broadening is directly linked with the electron density through electron impact parameter w_{FWHM}, by the following relation:

$$\Delta\lambda_{stark} = 2w_{FWHM}\left(\frac{n_e}{10^{16}\,\mathrm{cm}^{-3}}\right) \tag{4}$$

Once the Stark broadening is obtained, the electron density n_e can be estimated by using this relation (eq. 4) if the electron impact parameter w_{FWHM} is known, which can be found in the literature. Electron density in the plasma depends upon a number of experimental parameters, for example, laser energy, background gas, ambient pressure and characteristics of the target itself. However, it represents a temporal profile that follows an exponential decay as a function of plasma lifetime [7, 8].

5.1.2. Plasma temperature measurements

Plasma temperature can be determined by several spectroscopic methods, for example, the line-pair intensity ratio method, Boltzmann plot, line-to-continuum ratio method, etc. One method may be more suitable than others under specific conditions. For example, diagnostics

of the early-state plasma line-to-continuum ratio method is more suitable because during initial few hundred nanoseconds, both continuum and line intensities are of comparable strength. However, after a few microseconds, the continuum fades away and line intensities dominate in the spectrum; in such a situation, the line-pair intensity ratio or Boltzmann plot method would be more suitable. These methods are described as follows.

5.1.2.1. Line-pair intensity ratio method

Assuming that the plasma is in local thermodynamic equilibrium (LTE), the temperature of the plasma can be calculated through the intensity ratio of a pair of spectral lines of atom or ion of same ionization stage. In LTE, the level population supposedly obeys the Boltzmann distribution. Then the integrated intensity of a transition ($j \rightarrow i$) can be represented as [9]:

$$I_{ij} = n_i^s A_{ij} \tag{5}$$

Here, n_i^s represents the population density of species 's' in level 'i' given as

$$n_i^s = \frac{g_i}{U^s(T)} n^s e^{E_i/kT} \tag{6}$$

Therefore, intensity I_{ij} can be written as

$$I_{ij} = \frac{g_i A_{ij}}{U^s(T)} n^s e^{E_i/kT} \tag{7}$$

where g_i is the partition function of level 'i', A_{ij} represents the transition probability of $i \rightarrow j$ transition, n^s and $U^s(T)$ are total number density of species in the plasma and partition function of the species 's', respectively. E_i, k and T are energies of the upper level 'i', Boltzmann constant and plasma temperature, respectively.

Now, consider another spectral line of the same species but originated from a different transition, that is, $m \rightarrow n$. Such that the upper energy level is different (i.e. $E_i \neq E_m$) and the lower energy level may or may not be the same. By taking intensity ratio of these two spectral lines, the plasma temperature can be calculated as follows:

$$\frac{I_{ij}}{I_{mn}} = \frac{\frac{g_i A_{ij}}{U^s(T)} n^s e^{E_i/kT}}{\frac{g_m A_{mn}}{U^s(T)} n^s e^{E_m/kT}} \tag{8}$$

Rearranging

$$T = \frac{E_i - E_m}{k \ln\left(\frac{I_{mn} A_{ij} g_i}{I_{ij} A_{mn} g_m}\right)} \tag{9}$$

It is advisable to choose lines that are as close in wavelength and as far in upper-level energy as possible. It will limit the device response variation in measurement of spectral line intensities. Assuming that the experimental error influences only intensities of the spectral lines, error in the temperature measurement is given as [10]

$$\frac{\Delta T}{T} = \frac{kT}{\Delta E} \frac{\Delta R}{R} \tag{10}$$

Here, $\Delta E = E_i - E_m$ energy difference between upper energy levels and R measures the intensity ratio, that is, $R = I_{ij} / I_{mn}$. ΔR is the uncertainty associated with ratio and ΔT is the corresponding uncertainty in temperature measurement.

5.1.2.2. Boltzmann plot method

Boltzmann plot is a reliable method for calculation of plasma temperature that has been trusted by many researchers in the latest literature.

The emission intensity of a spectral line is represented as [11]

$$I_{ij} = \frac{hc}{4\pi} \frac{A_{ij} g_i}{\lambda_{ij} U(T)} n e^{-E_i / kT} \tag{11}$$

Here, h, c, k, T and $U(T)$ are the Plank's constant, speed of light, Boltzmann constant, plasma temperature and partition function, respectively, whereas A_{ij}, g_i, E_i, λ_{ij} and n are the transition probability, degeneracy of upper level, upper-level energy, emission wavelength and total population density of the emitting species, respectively.

Taking natural logarithm and re-arranging the eq. (17), we obtain

$$\ln\left(\frac{I_{ij}\lambda}{g_i A_{ij}}\right) = \frac{-E_i}{kT} + \ln\left(\frac{hcn}{4\pi U(T)}\right) \tag{12}$$

This is the equation of a straight line that arises as a result of plot between $\ln\left(\frac{I_{ij}\lambda}{g_i A_{ij}}\right)$ and upper-level energy E_i. The slope of this plot is equal to $-1/kT$. From this slope, plasma temperature 'T' can easily be estimated [12, 13]. The further apart the upper-level energies of the selected lines,

the better would be the measurement of the slope. The Boltzmann plot method is considered to be more precise for using several lines that averages out uncertainties involved in measurement than the intensity ratio method, which makes use of a pair of emission lines only [9]. The value of plasma temperature depends upon laser–target interaction, laser energy and characteristics of the ambient environment. However, it shows exponential decay during the lifespan of laser-induced plasma [7, 8].

5.2. Electrical diagnostics

A number of electrical diagnostic tools are used to characterize the laser-induced plasma. Few of them are briefly discussed in this section.

5.2.1. Langmuir probe

The Nobel laureate Irving Langmuir has invented the Langmuir probe to determine the electron temperature, density and the space potential V_{sp} in cold low-density plasmas. The local plasma parameters can be measured using stationary or slow time-varying electric (and/or magnetic) fields to collect or emit charged particles from the plasma. The charge particles, electrons, ions or both, are collected through the electric field established between the bulk plasma and the metallic surface of the probe. The simplest Langmuir probe consists of a metallic electrode, a bare wire or metal disk, with well-defined dimensions such as planar, cylindrical or spherical as shown in Figure 5. Langmuir probe is electrically biased with respect to a reference electrode to collect electron and/or positive ion currents. The dimensions of the probe as length, diameter and the thickness (or spatial extension) of the plasma sheath attached to the collecting surface play an important role in the collection of charge particles [14, 15].

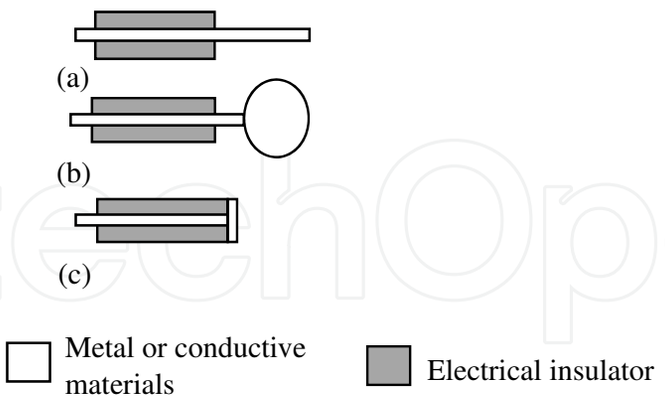

Figure 5. Schematic diagram of the Langmuir probe with different dimensions (a) cylindrical, (b) spherical and (c) planar

The metallic probe is immersed into the plasma and a potential V_p is provided to the probe using an external circuit, which bias the probe $V = V_p - V_{sp}$ with respect to the local space plasma potential V_{sp}. The drained current called probe current $I_p = I(V_p)$ for different probe potentials V_p is utilized to measure the different plasma parameters via voltage–current (IV) characteristic

http://dx.doi.org/10.5772/61784

curves [14]. Figure 6 shows typical voltage–current (IV) curve of the Langmuir probe. The potential V_{sp} presents the localized electric potential at the point within plasma where the probe is immersed. As the probe does not emit particles, the drained current 'I_p' is the combination of ion current 'I_i' and electron current 'I_e', that is, '$I_p = I_i + I_e$'.

For very negative bias voltages where V_p is much less than V_{sp} (i.e. $V_p << V_{sp}$ at the left of point A as shown in Figure 6), the electrons are repelled, while ions are attracted by the probe. In this region, the characteristic curve is designated as the 'ion accelerating region'. The probe potential is sufficiently negative that only positive ions contribute to the probe current. The drained ion current from the plasma is limited by the electric shielding of the probe and I_p decreases slowly. The current $I_p \simeq I_{is}$ is the denominated ion saturation current.

The voltage corresponding to zero value of current is termed as the 'floating potential'. The bias potential V_F where $I_p = 0$ is the floating potential (point B) where the contributions of the ion and electron currents are equal.

After the floating potential, the *I–V* trace takes a sharp turn upwards. The bend is also referred to as the 'knee'. At this point, probe has the plasma potential. In the region, where V_p is much higher than V_{sp} (i.e. $V_p \gg V_{sp}$ at the right of point C as shown in Figure 6), the ions are repelled and the electrons are the attracted charges. In this case, the electrons are responsible for the electric shielding of the probe, and $I_p \simeq I_{es}$ is called the electron saturation current. As the positive bias is increased on the probe, eventually the collected electron current reaches a saturated value, that is, maximum electrons collected by the probe [14].

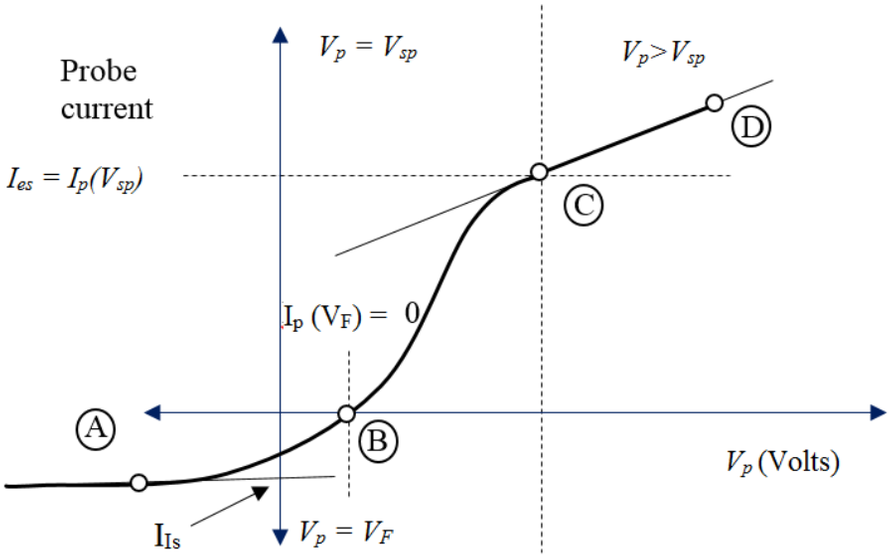

Figure 6. Typical voltage current (IV) curve of the Langmuir probe

For the qualitative interpretation, an idealized non-equilibrium collisionless, Maxwellian and unmagnetized plasma conditions are considered. Under the Maxwellian distribution, current density follows the Boltzmann law [16]:

$$J = J_o \exp(-eV / kT_e) \tag{13}$$

where '*k*' is the Boltzmann constant, '*T*' is the temperature and '*J*' is the current density at any potential '*V*' and J_o is the current density at zero potential:

$$I = I_o \exp(-eV / kT_e) \tag{14}$$

If 'T_e' is the electron temperature, 'V_a' is the applied biasing voltage; 'I_p' is the probe current at any biasing voltage and 'I_o' is the probe current at zero biasing:

$$I_p / I_o = \exp\left(eV / kT_e\right) \tag{15}$$

$$\begin{aligned} \ln(I_p / I_o) &= eV / kT_e \\ T_e &= eV / k.1 / \ln(I_p / I_o) \end{aligned} \tag{16}$$

Electron density of the laser-induced plasma can be calculated by the relation

$$n_e = I_o / A_e.[m_e / 2\varepsilon_0 kT_e]^{1/2} \tag{17}$$

where T_e is the electron temperature; I_o is the probe current at $V_a = 0$; A_e is the probe surface area; n_e is the electron density; m_e is the mass of electron; k is the Boltzmann constant; and ε_0 is the permittivity of free space.

Debye's length can be calculated as

$$\lambda_D = [\varepsilon_o kT_e / e^2 n_e]^{1/2} \tag{18}$$

Plasma frequency can be calculated as

$$\omega_p = (n_e e^2 / \varepsilon_o m_e)^{1/2} \tag{19}$$

5.2.2. Faraday cup

Faraday cup (FC) is a metal cup with small aperture and a deep collector, which is designed to collect charged particles. When charged particles hit the metal, the metal gains a small net charge. The metal can then be discharged to determine a small current equivalent to the number of impinging charged particles as ions or electrons. A Faraday cup is used as a

measurement tool for charged-particle-beam parameters such as current and current density profile. In the laser-induced plasma, the FC is used to measure the charged-particle parameters such as charge particle density, energy (using time of flight technique), the plasma angular distribution and distance charge dependence during the plasma-free expansion into the vacuum [17, 18].

The typical FC configuration is schematically shown in Figure 7, which mainly consists of two major parts: an inner cup for the charged particle collection and the grounded shield to measure the current I_c produced by the primary charged particle striking the cup. The electric current in the FC depends on the incident particle beam [19, 20].

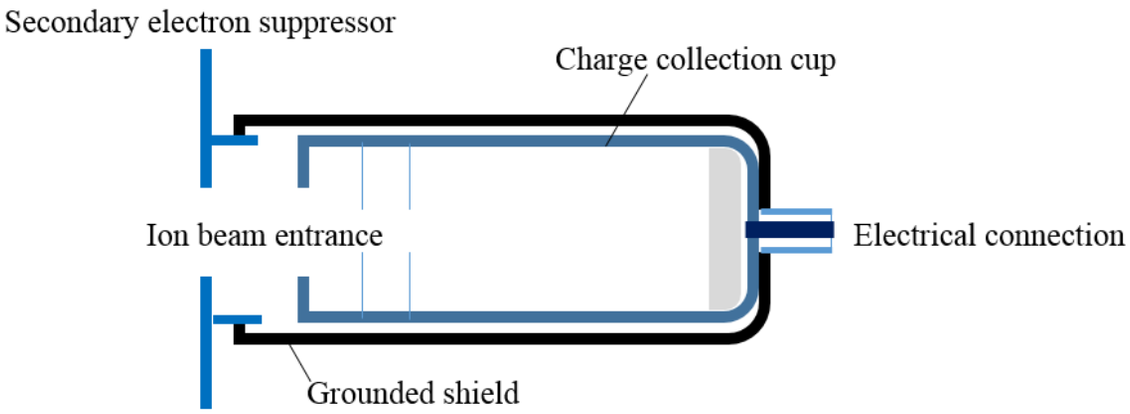

Figure 7. Schematic sketch of the Faraday cup

A bias voltage is applied to the cup to prevent secondary emission and electrons from escaping. The FC is connected to the measuring device as ammeter or oscilloscope to display the signal across a resistor from the conducting lead to ground [21, 22].

5.2.3. Scintillators and photomultiplier tubes

Radiation detectors play an important role in the non-destruction inspection and analysis in different field of studies. Photomultipliers are used to identify low-energy photons in UV–Vis range; high-energy photons (X-rays and gamma rays) and ionizing particles are identified using scintillators. The combination of photomultiplier tube and scintillator is one of the effective tools for the non-destruction characterization, which has several advantages such as fast time response, high detection efficiency, wide detection area and availability of different types of detective materials over number of other detection methods. A photomultiplier with scintillator converts radiations to an electrical signal, which is amplified to a useful level by emission of secondary electrons [23]. Due to high selectivity of photomultiplier tube, it is used to characterize the X-ray radiations ranging from 10 to 10 keV (soft and hard X-rays) [24, 25].

Figure 8 shows the schematic sketch of the photomultiplier system, which consists of a photocathode (scintillator) to convert radiation flux into electron flux, electron-optical input system to focus and accelerate the electron flux, electron multiplier comprises a series of

secondary-emission electrodes (dynodes) to amplify the electric signal and an anode to collect the electron flux from the multiplier and displays the output signal.

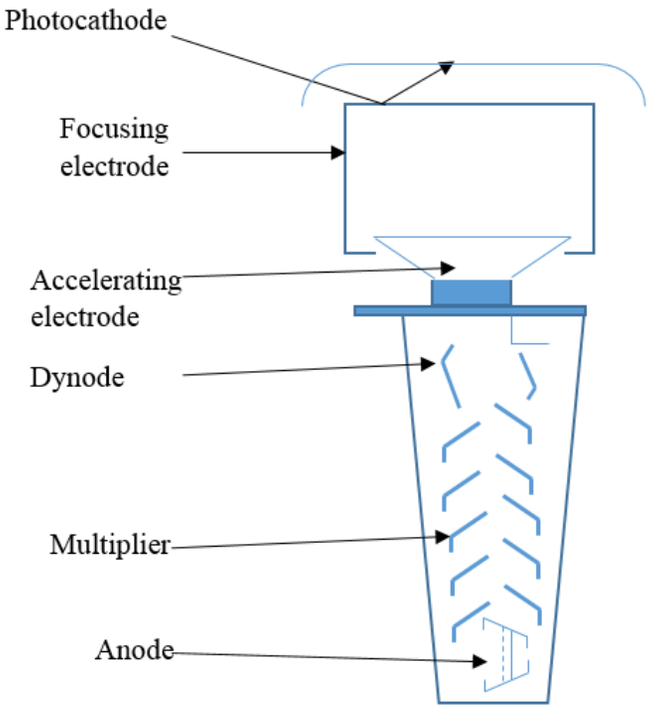

Figure 8. Schematic sketch of the photomultiplier system

The two fundamental phenomena to operate a photomultiplier are photoemission and secondary emission. Photoemission is due to a fraction of the incident photons that impart all their energy to bonded electrons of the photocathode material, giving some of the sufficient energy to escape, which are then amplified by dynodes and displayed as the output [23, 26].

5.3. Solid-state detectors

Solid-state nuclear track detectors (SSNTDs) are used to detect and estimate the energy of the charged particles in various disciplines. The solid-state nuclear track detection is an important and useful method to detect charged particles with energy ranging from tens of kilo-electron volts up to few hundred mega-electron volts. For instance, the detector of CR-39 is suitable for the detection of protons, deuterons and alpha detection due to high sensitivity of CR-39 material towards these particles. Once the SSNTD material is exposed to charged particles, these particles leave narrow damage trails on their passage through SSNTDs [27]. These damage trails represent regions of enhanced chemical activity as compared with bulk material due to disorders in the structure caused by the charged particles, which in turn are associated with large free energy. These trails are too small to be seen even with the help of a microscope. Therefore, the exposed detector material containing damage trails is subjected to the etching process in next stage to remove the material from the track.

To make the tracks visible, the exposed detectors are etched in the chemical solution to a certain temperature and for specific time. The etched detectors were then examined using an optical microscope or scanning electron microscope [28]. An optical micrograph for the carbon ions on the CR-39 material is shown in Figure 9.

On treating with suitable chemical reagents, the detector material along the damage trails interact much faster as compared with the undamaged bulk material. The resulting etch pits can be approximated by geometrical cones with the damage trails as axes. The study of etch-pit geometry and determination of the range of particles in the detector provides the identification of the particles creating the tracks and energies of particles [27].

The diameter of the etched tracks is used to evaluate the energy of the ion using diameter energy relationship given as

$$D = 1.8409E^{0.1624} \tag{20}$$

where D is the track diameter in micrometers and E is the energy in kilo-electron volt [29].

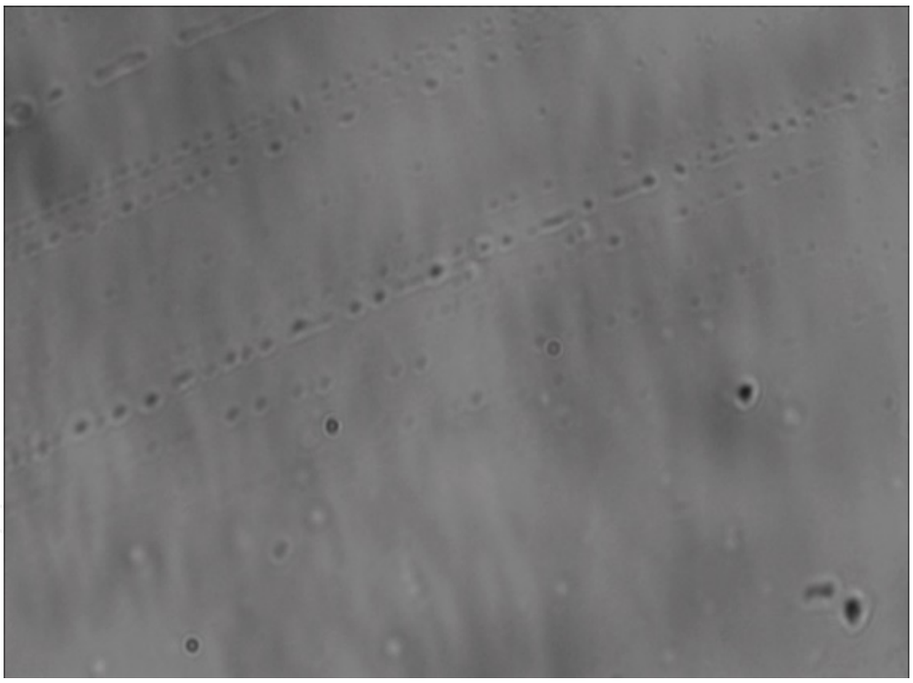

Figure 9. Optical micrograph of carbon ions track on CR-39 material

6. Applications of laser-induced plasma

Due to versatility of laser-induced plasma, it has been found to be suitable for numerous applications in various fields of science and technology. The utility of powerful lasers in

remote, physically inaccessible locations makes it a special tool for applications in hostile environments. Laser-induced plasma has been utilized for lateral and depth elemental analysis, thin-film deposition, X-ray production, ion production, identification of materials, etc. Further details on applications of different aspects of laser-induced plasma are described in the following sections.

6.1. Laser-induced breakdown spectroscopy

The optical emission spectroscopy of laser-induced plasma is named as laser-induced breakdown spectroscopy (LIBS) or sometimes laser-induced plasma spectroscopy (LIPS). It is a powerful and versatile analytical technique for elemental analysis, which could be utilized for an enormous range of materials. Spectral features such as emission lines, peak intensity and integrated intensity, etc. are used for the determination of elemental concentration of the target or discriminate one material, organic or inorganic, from another through their unique spectral signatures. The basic set-up of LIBS is very simple (Figure 10); however, for higher signal intensities and lower limit of detections (LOD), double-pulse configuration of LIBS is preferred that has two variants, that is, collinear and orthogonal as shown in Figure 11. Reheating or preheating modes of operation can be utilized in both of these configurations. In the reheating mode, the laser pulse 1 ignites plasma plume, whereas laser pulse 2 (after a certain time delay) further excites plasma species to obtain larger amount of radiations. While in preheating mode, the laser pulse 1 heats the atmosphere above target surface and lets the plasma, generated by laser pulse 2, expand in hot and rare ambience.

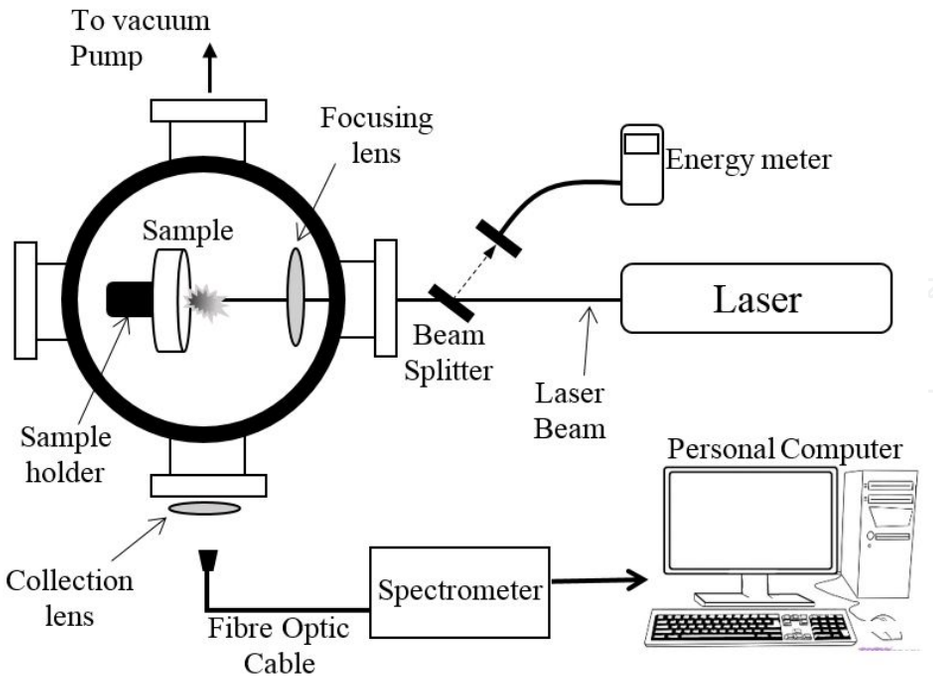

Figure 10. Schematic diagram of a typical laser-induced breakdown spectroscopy set-up

http://dx.doi.org/10.5772/61784

LIBS provides a huge advantage of requiring no specific sample preparation procedure to follow. Ideally, it can be utilized for solid, liquid and gaseous types of materials. Unique features of LIBS are stand-off and remote analyses that are typically useful when dealing with hazardous materials, toxic environments and humanly inaccessible locations. These characteristics are unique for LIBS because other chemometric techniques do not offer such utility. In the following sections, we discuss versatile applications of LIBS in various fields of science in the recent years.

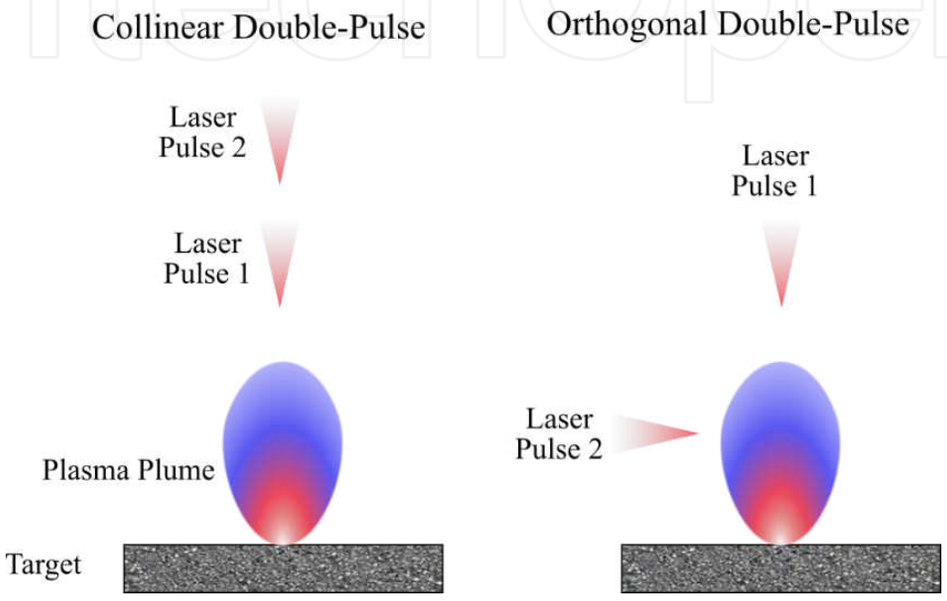

Figure 11. Two different modes of double-pulse laser-induced breakdown spectroscopy (DP-LIBS)

6.1.1. Geochemical applications

LIBS has proved to be useful in *geochemical* studies. The spectral signatures obtained from laser-induced plasma of targets have made investigations of geological materials possible. It has been taken up as a new technique for geological studies to determine the origin of petrogenetically important minerals and archeologically important rocks and stones on the basis of their physical and chemical properties. It includes not only the typical elemental measurements but also material identification with and without using machine-learning software [30-34].

With the capability of highly localized analysis (on the scale of μm), LIBS has made the spatial profiling of minerals possible in geological samples. Prochazka et al. [35] utilized LIBS for 3D profiling of minerals in geological samples performed at a resolution as high as 100 μm. They practised the advantage of no pretreatment of samples and found very good results.

6.1.2. Environmental applications

Another aspect of LIBS applications is *environmental studies*. It has widespread applications in environmental sciences for real-time elemental detection and analysis outside the laboratory. Its portability, simple execution, no requirement of sample preparation and simultaneous

multi-element identification are attractive attributes for on-site analysis in terms of environmental health and safety. It covers a wide range of samples from industrial waste water to aerosols in the air.

LIBS has been successfully used for the identification and quantification of various pollutants and elements including carbon (C) in samples of diverse nature and origin [36-39]. Carbon is a good indicator of CO_2 gas in the environment, which is a greenhouse gas and influences the climate change. Since CO_2 cycles between atmosphere, vegetation and soil, it is quite possible that it increases the content of C in terrestrial carbon sinks, for example, soil. Therefore, the increase in the C content of terrestrial carbon sinks is an indicator of increasing CO_2 in the environment. Several studies have been performed that demonstrate the inherent advantages and capabilities of LIBS for quantification of the C content in soil from various origins [40-42]. Martin *et al.* [43] successfully attempted to differentiate the organic and inorganic C in the selected set of soil samples by the application of chemometric techniques of partial least squares (PLS) and principal component analysis (PCA) on LIBS spectra. By obtaining the correct signal intensity, linearity of their calibration curves significantly improved, that is, indicator of improvement accuracy of measurements. Nguyen *et al.* [44] determined the C concentration as an indicator of CO_2 greenhouse gas. The challenge regarding overlapping of C emission lines was handled by optimizing the time window of data collection for minimum broadened lines to mitigate interference effects. An accuracy of 95% was ensured in measurements of C in forest soils, wetland soils and sediment samples.

In addition to greenhouse gases, heavy metals are of major concern for human health and safety. The presence of toxic heavy metals like arsenic, lead, antimony, zinc and cadmium in natural resources of the environment, for example, water, soil, air etc. or synthetic products that come in direct human contact, such as paint, are of risk for living organisms. Because of the toxicity of Pb, which could be poisonous for the human body [45], its detection and achieving low limits of detection have always been the matter of interest. Analysis of liquid samples with LIBS is challenging; short lifetime of plasma, liquid–laser coupling and splashes resulting from plasma shockwaves raise the difficulty of LIBS measurement and increase the limit of detection for liquid samples. However, new techniques for LIBS are improving the analysis of liquid samples. Järvinen *et al.* [46] incorporated evaporation pre-concentration for the measurement of Zn and Pb in water and at limits of detection as low as 0.3 and 0.1 ppm, respectively.

6.1.3. Agricultural applications

LIBS has a prominent potential for agricultural studies. Portability and no sample preparation features again provide LIBS an advantage over conventional analytical techniques. Soil, crops, plants, fruits, grains and irrigation water can be tested in field. Although the portable systems for agricultural applications are not very mature, the pace of technological advancement suggests that some decent portable LIBS systems for a variety of applications would be available soon.

LIBS has successfully been utilized for agricultural studies from various aspects. Nutrients and minerals in the soil are of great importance from agricultural point of view. There are many

studies referring to the employment of LIBS for measurement of macro- and micronutrients in soil and crops. Naturally, organic samples are not very homogeneous in elemental composition. It is sometimes difficult to analyse heterogeneous samples with LIBS because it only provides information about a highly localized region on the sample surface. The determination of Fe, Mn, Mg, Ca, Na and K in heterogeneous soil samples was performed by Nguyen [44] by using laser ablation–LIBS (LA–LIBS) without sample preparation. Unnikrishnan *et al.* [47] demonstrated the measurement of trace amounts of nutrients Cu, Zn and Ca in soil samples with limits of detection of 4.8, 4.4 and 6 ppm, respectively. In addition to mare elemental analysis, a recent publication by Ferreira *et al.* [48] shows that LIBS can potentially be effective in determination of pH of soil.

LIBS has been employed for studying diverse plants for practical applications and for exploration and development [49-51]. It is well known that the deficiency of macro-/micronutrients can adversely affect the crop yield and degrade the nutritious quality of the product. Therefore, monitoring of essential elements in crop plants, fruits and vegetables is vital for maintaining the nutritional status and food security. Numerous studies can be listed in which LIBS is featured as an investigation tool for nutritious quality of diverse range of organic samples. For instance, Arantes de Carvalho *et al.* [52] studied macro- (Ca, Mg, P) and micronutrient (Cu, Fe, Mn and Zn) concentrations in a variety of crop samples that include sugarcane, soy, citrus, coffee, maize, eucalyptus, mango, bean, banana, lettuce, brachiaria, pearl millet, grape, rubber tree and tomato. Kim *et al.* [53] investigate the quantity of macronutrients (Mg, Ca, Na and K) in spinach and rice samples and apply discriminatory operations upon LIBS spectra to discriminate the samples contaminated with pesticides from clean ones. LIBS has also been utilized for the determination of toxic heavy metals and contaminations residing on the surface of fruits because of environmental pollution and pesticide sprays [54, 55]. The list of publications regarding LIBS applications for investigations of agricultural products encompassing diverse variety of samples is long. One can simply deduce its applicability in almost all parts associated with agriculture, ranging from irrigation water to ripe crops, fruits and vegetables.

6.1.4. Stand-off and remote applications

Stand-off and remote analysis capabilities are unique for LIBS. In stand-off application, a powerful laser pulse is fired at a distant (approximately several meters) target and emissions from the microplasma at the target surface are collected through a telescope. Schematic diagram of a typical stand-off LIBS system is provided in Figure 12. In remote studies, a fibre-optic probe is commonly utilized to reach remote and humanly inaccessible locations. This probe delivers the laser to the target and transfers the plasma radiations from target to the spectrometer back in the system. Schematic illustration of a typical remote LIBS system is depicted in Figure 13. Portability of LIBS system has elevated the potential of LIBS capability in the investigation of quarantined regions, potentially hostile and physically inaccessible locations. Applications of stand-off and remote LIBS can be found in identification of biomaterials at far distance, investigation of deep sea objects, studying radioactive and explosive materials from a safe distance, monitoring the composition of alloys in production line, Mars and exploration, etc.

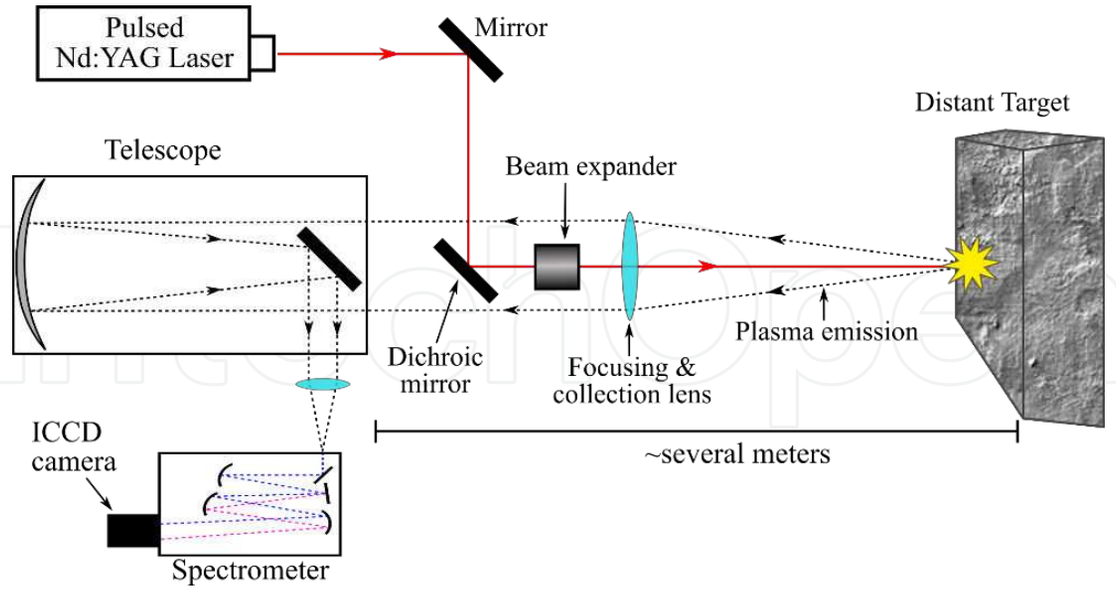

Figure 12. Schematic illustration of a typical stand-off LIBS system

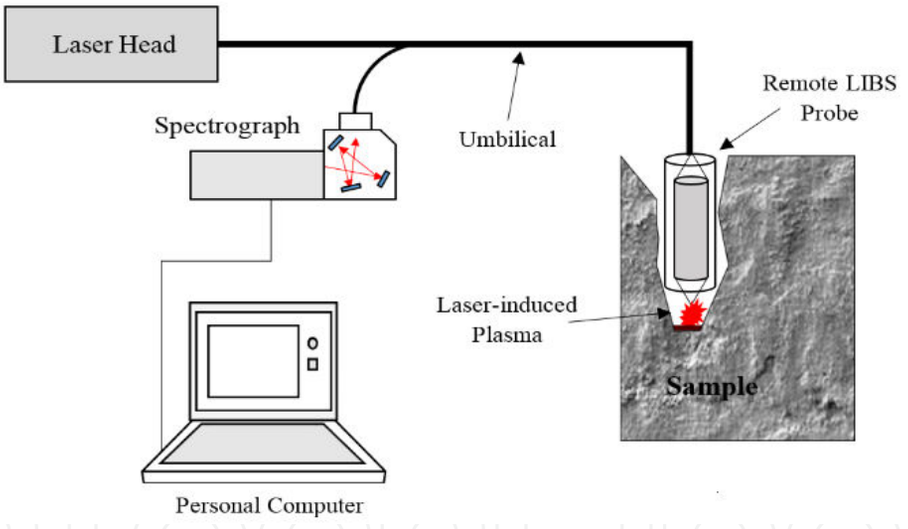

Figure 13. Schematic illustration of a typical remote LIBS system

At a distance of ~6.2 m, Vítková *et al.* [56] performed LIBS analysis on a variety of biological samples that included mortar, sea shell, human tooth, swine bone, soil pellet and a brick. Each of these samples was classified on the basis of their spectral signatures by complementing LIBS with supervised machine-learning methods, such as linear discriminant analysis (LDA) and artificial neural networks (ANN). In another study, Vítková *et al.* [57] demonstrated the LIBS-based discrimination of historically important bricks according to their archaeological localities with the help of LDA at a stand-off distance of ~6.2 m. Another application of stand-off LIBS is presented for the analysis of soil and vegetation powders for studying the content of heavy metals and toxic trace elements in targets [58].

An interesting underwater application of stand-off LIBS is demonstrated by Fortes *et al.* [59]. To test the feasibility of underwater LIBS at a stand-off distance of 0.8 m from sensor to the target deeply submerged in the water, fundamental investigations were performed. A similar study has reported [60] the application of remote LIBS for studying underwater shipwreck. In such applications, the advantage of remote over stand-off approach is that the laser beam interaction with ocean water is minimal and the laser energy losses are likewise minimum. However, the advantage of stand-off approach is that it is not required to bring the LIBS probe to the target in deep waters, rather, measurements can be taken from far.

Stand-off LIBS is capable of investigating nuclear materials from a safe distance, for instance, Gong *et al.* [61] has demonstrated the investigations made on cerium oxide (CeO_2) and potassium chloride (KCl) at a stand-off distance of 1.45 m through the protection shield. Stand-off LIBS is particularly suitable for industrial applications like real-time monitoring of product quality in production line without interfering the production process [62].

LIBS has gained popularity among the geologists since the NASA has equipped the Curiosity Mars rover with a ChemCam LIBS system. A field test of this system with a remote analysis probe was published as a meeting abstract [63]. The ChemCam LIBS system has proved useful and reliable in Mars exploratory mission since the Curiosity has landed the surface of Mars in year 2012 [64].

6.2. Pulsed laser deposition

Pulsed laser deposition is a versatile technique. It makes use of the laser's ability to ablate and excite almost every type of material and, therefore, has been utilized to deposit an extensive range of thin films may it be metallic, polymeric or composite.

A high-power laser pulse, typically $\geq 10^8$ W/cm^2, is utilized to evaporate and ionize the material into a plasma plume that expands in the ambient environment perpendicular the target surface. This evaporated and highly accelerated material is collected on an appropriately positioned substrate upon which it condenses and grows a thin film. The size and expansion velocity of the plasma plume depend largely upon nature and density of the ambient atmosphere along with laser pulse duration and irradiation. The plasma plume has found to expand with velocities of the order of 10^6 cm/s under vacuum conditions (~10^{-6} mbar) for typical laser fluences ~10^9–10^{10} W/cm^2 and increases for higher fluences. Plume dimensions and expansion velocity are also inverse functions of the ambient pressure and time [65, 66]. When the plasma species strike surface of the substrate with such high velocities, sufficient adhesion is obtained to keep particles sticking with the surface for gradual growth of the film. The film growth and quality depend upon characteristics of substrate, substrate temperature and energy of the plasma species, that is, atoms, ions and clusters striking the surface of substrate that in turn depends upon laser parameters. Surface morphology and texture of thin films are strongly influenced by substrate temperature, nature and pressure of the ambient gas. By controlling the ambient atmosphere, we can actually control mechanical, optical, surface morphological properties of the deposited thin film. The choice of laser and laser parameters are vital for PLD. The selection of wavelength and energy of laser depends upon the coupling efficiency with

target material to be used. Nanosecond Nd:YAG and excimer lasers are the most widely utilized lasers for PLD as found in the published literature.

PLD is principally a simple technique and versatile in terms of utilizing target and substrate materials. A typical PLD arrangement is schematically illustrated in Figure 14. Laser ablation is considered to be a stoichiometric phenomenon, which means that plasma plume has the same composition as that of the target that is delivered onto the substrate surface as a thin film. It is normally referred to as 'stoichiometry transfer' from target to film on substrate surface that is difficult to achieve with other techniques. It, therefore, permits the control of thin-film composition by appropriate selection of target composition. Multilayers of different materials can be deposited on a single substrate by using multiple targets during the PLD procedure. Since only small substrate areas (typically ~1 × 1 cm^2) can be targeted by the laser-induced plasma, it allows the preparation of complex samples enriched with isotopes for laboratory-scale research purposes. Being a short-pulsed phenomenon makes PLD a flexible operation, because operational parameters can be varied from pulse to pulse according to the requirement of the application.

Despite numerous advantages of the PLD technique, it is not yet well adopted in the industrial manufacturing process because of the uncontrolled plasma process and small-area deposition. In addition, the deposition may not be of uniform thickness because of strong forward peaking nature of the laser-induced plasma. However, it has gained popularity among the scientists who are convinced and exploring its enormous potential in laboratories and discovering new possibilities and procedures for extensive applications in diverse fields of science and technology. Amorphous, polycrystalline, epitaxial thin films can be grown, depending on the nature of the substrate and its temperature. There are a large number of applications in which PLD has shown great promise, for example, photovoltaics, superconductor technology, nanostructured thin films, optical coatings, etc.. Following is given a brief review of versatile applications of PLD.

PLD has been found to be very suitable for deposition of thin films for *photovoltaic* applications. Sekiguchi *et al.* [67] were perhaps the first to demonstrate the use of PLD for epitaxial growth of CZTS films on GaP substrates heated at 350–400 °C. Stoichiometric crystalline thin films with an appropriate optical band gap of ~1.5 eV were observed. However, the first-ever publication about Sn-rich CZTS thin film deposition by PLD, particularly for solar cell applications was reported by Moriya *et al.* [68]. Films showed an optical band gap of ~1.5 eV, consequently prepared solar presented a conversion efficiency of 1.74% for an active area of 0.092 cm^2.

Pulsed laser deposition has also found application in depositing high-quality superconducting thin films. Superconductivity has found to be thickness dependent; therefore, precise control of thin films is crucial. Here, PLD provides an advantage of controlled growth of thin films through variation in experimental parameters [69, 70], which can improve the quality of thin films in individual applications. There are many recent studies found in literature that demonstrate the exploration of experimental parameters of PLD for diverse types of high-quality superconducting thin films. Oshima [70] report the deposition of $LiTi_2O_4$ thin films of various thicknesses by employing the PLD method using krypton fluoride laser (KrF) excimer

http://dx.doi.org/10.5772/61784

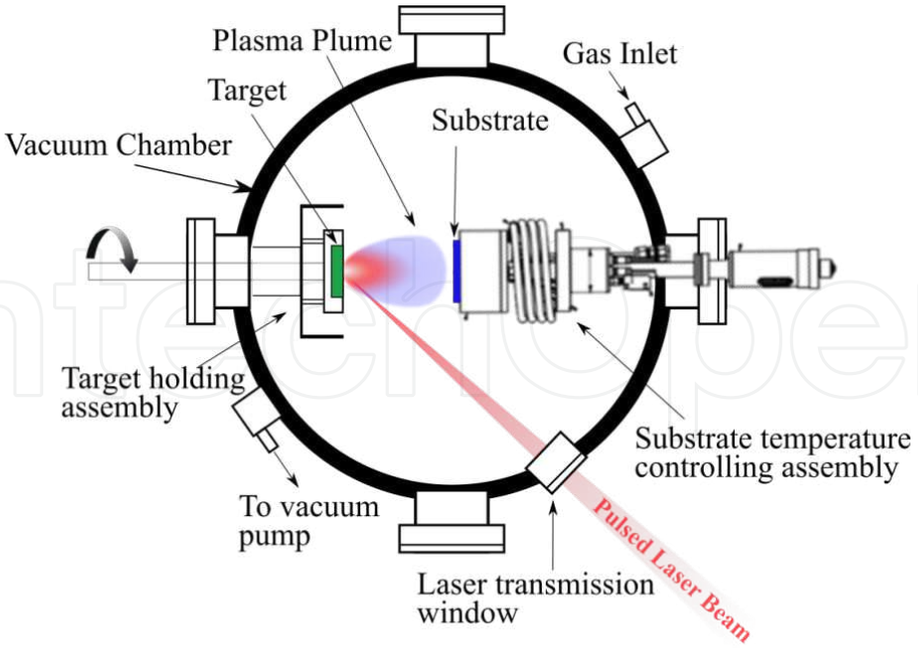

Figure 14. Schematic illustration of pulsed-laser deposition system

laser. Superconducting transition was observed around 12 K at a film thickness of 9 nm. One of the benefits of PLD method is that quality and thickness of thin films can be controlled by varying deposition time, growth rate (determined by pulse repetition rate) and substrate temperature during the film growth [69, 70].

PLD method is highly suitable for growing *composite thin films* of a wide range of materials over diverse substrates. Sharma *et al.* [71] report on composite thin films $0.9BiFeO_3$-$0.1YCrO_3$ on Pt, TiO_2, SiO_2 and Si substrates by sequential deposition of $BiFeO_3$ and $YCrO_3$ targets by the PLD method. Consequently obtained thin films represented fine, particle-free smooth surfaces with a crystal structure as a mixture of $BiFeO_3$ and $YCrO_3$ crystals. Chowdhury *et al.* [72] deposited SnO_2-Fe_2O_3 composite thin films by the PLD method with the aim to investigate structural, morphological, optical and electrical properties that revealed their suitability for optoelectronic applications.

An interesting possible application of PLD can be the coating of surgical instruments with antimicrobial composite thin films. Several studies have demonstrated the growth of antifungal and antibacterial composite thin films on various substrates. For instance, Ag-SiO_2 antibacterial composite thin films were grown on Si (111) substrate by the PLD method using KrF Excimer laser [73] at room temperature in the oxygen environment. In another study, Pradhaban *et al.* [74] demonstrated the deposition of antibacterial Ag:ZrO_2 composite films on stainless steel substrates by the PLD technique using Nd:YAG laser. Similary, Eraković *et al.* [75] utilized PLD to grow antifungal Ag:HA (hydroxyapatite) composite thin films on titanium (Ti), anodized Ti and Si (111) substrates.

PLD is still a laboratory-scale method for thin-film deposition. Large amount of data published on investigation of the PLD method for a variety of applications is an evidence of intensive

efforts being made by the scientists. However, it will take time to see the PLD method being used for industrial-scale applications.

7. Conclusions

This chapter encompasses fundamentals of laser-induced plasma from laser–matter interaction to radiation emission from plasma and deposition of the ablated material on a distant substrate. LIP is a rapid process and fairly complex in nature. It starts with absorption of pulsed-laser energy by the material that breaks it down and evaporates it in the form of plasma that eventually decays after few tens of microseconds. During its lifetime, the plasma temperature, particle density and continuum and line emissions show temporal fluctuations. Characteristics and emissions of laser-induced plasma strongly depend upon laser parameters, nature of the target and ambient conditions. There are several methods used for estimation of plasma parameters based on spectroscopic data. Among them, the Boltzmann plot method for plasma temperature measurements and the Stark broadening method for estimation of electron density are the most commonly used methods. Besides spectroscopic diagnostics, the most well-known electrical diagnostic tools include Langmuir probe, Faraday cups and scintillators and photomultipliers, which have been widely used to study plasma parameters, energy of charged particles and X-ray emissions from plasma, respectively. A physical method of measuring the density, energy and distribution of charged particles is the use of solid-state nuclear track detectors. By investigating the density and dimensions of the tracks produced on SSNTDs, the density, energy of the particles emitting at various angles of the plasma can be obtained.

Being a rich source of radiation and particle emission, LIP has found a variety of applications in diverse areas. Line emissions from the laser-induced plasmas inform about elemental composition of the material that has opened up several fronts of applications. It is termed as LIPS (laser-induced plasma spectroscopy). It has been utilized for numerous laboratory and in-field applications from food safety to explosive detection, soil studies to Mars exploration, archaeology to artefact studies, micro to bulk exploration and many more. The samples that could be studied with LIPS have virtually no limits, from solids to gasses and aerosols have been investigated that encompass organic materials to nuclear and explosive materials. In addition to spectroscopic investigations, the excited material of LIP has been utilized for thin-film deposition on a wide range of substrates for diverse applications. It is commonly termed as pulsed-laser deposition. Through PLD, films of various materials including conductors, insulators, dielectrics, in general, have been deposited on a variety of substrates. Deposition of complex hybrid and multilayer films, a combination of multiple materials, have also been successfully demonstrated. The quality, morphology and structure of films depend upon the ambient atmosphere and substrate temperature besides laser parameters.

Because of numerous intrinsic benefits of LIP for various applications over other conventional techniques, some commercial products, specifically LIPS systems, can be seen in the market. However, the uncontrolled nature of LIP hinders its wider deployment for industrial appli-

cations. Most of the potential applications are still in infancy and are being explored at the laboratory level. Keeping in mind the current pace of advancement in technology and enormous potential of LIP, in near future, we can expect to see some products in the market that are based on LIP for innovative applications.

Author details

Kashif Chaudhary*, Syed Zuhaib Haider Rizvi and Jalil Ali

*Address all correspondence to: kashif@utm.my

Laser Center, Ibnu Sina Institute for Scientific & Industrial Research (ISI-SIR), Universiti Teknologi Malaysia (UTM), Malaysia

References

[1] Wu, B. and Shin, Y.C. (2006), Modeling of nanosecond laser ablation with vapor plasma formation. Journal of Applied Physics. 99(8): 084310.

[2] Bäuerle, D.W., Laser Processing and Chemistry. 2011: Springer Berlin Heidelberg.

[3] Phipps, C., Laser ablation and its applications. Vol. 129. 2007, New Mexico: Springer.

[4] Harilal, S.S., Freeman, J.R., Diwakar, P.K., and Hassanein, A., Femtosecond laser ablation: fundamentals and applications, in Laser-Induced Breakdown Spectroscopy. 2014, Springer. p. 143-166.

[5] Leitz, K.-H., Redlingshöfer, B., Reg, Y., Otto, A., and Schmidt, M. (2011), Metal ablation with short and ultrashort laser pulses. Physics Procedia. 12: 230-238.

[6] Singh, J.P. and Thakur, S.N., Laser-Induced Breakdown Spectroscopy. 2007: Elsevier Science.

[7] Hegazy, H., Abd El-Ghany, H.A., Allam, S.H., and El-Sherbini, T.M. (2014), Spectral evolution of nano-second laser interaction with Ti target in nitrogen ambient gas. Applied Physics B. 117(1): 343-352.

[8] Aragón, C., Aguilera, J.A., and Manrique, J. (2014), Measurement of Stark broadening parameters of Fe II and Ni II spectral lines by laser induced breakdown spectroscopy using fused glass samples. Journal of Quantitative Spectroscopy and Radiative Transfer. 134: 39-45.

[9] Miziolek, A.W., Palleschi, V., and Schechter, I., Laser Induced Breakdown Spectroscopy: Fundamentals and Applications. 2006: Cambridge University Press.

[10] Harmon, R.S., DeLucia, F.C., McManus, C.E., McMillan, N.J., Jenkins, T.F., Walsh, M.E., and Miziolek, A. (2006), Laser-induced breakdown spectroscopy – An emerging chemical sensor technology for real-time field-portable, geochemical, mineralogical, and environmental applications. Applied Geochemistry. 21(5): 730-747.

[11] Cremers, D.A. and Radziemski, L.J., Handbook of Laser-Induced Breakdown Spectroscopy. 2006: Wiley.

[12] Aragón, C. and Aguilera, J.A. (2008), Characterization of laser induced plasmas by optical emission spectroscopy: A review of experiments and methods. Spectrochimica Acta Part B: Atomic Spectroscopy. 63(9): 893-916.

[13] Unnikrishnan, V., Mridul, K., Nayak, R., Alti, K., Kartha, V., Santhosh, C., Gupta, G., and Suri, B. (2012), Calibration-free laser-induced breakdown spectroscopy for quantitative elemental analysis of materials. Pramana. 79(2): 299-310.

[14] Conde, L. (2011), An introduction to Langmuir probe diagnostics of plasmas. Madrid: Dept. Física. ETSI Aeronáut ngenieros Aeronáuticos Universidad Politécnica de Madrid. 1-28.

[15] Merlino, R.L. (2007), Understanding Langmuir probe current-voltage characteristics. American Journal of Physics. 75(12): 1078-1085.

[16] Tufail, K. (2008), Magnetic field effect on electron emission from plasma, Master of Science Thesis, University of Engineering and Technology.

[17] Lorusso, A., Velardi, L., and Nassisi, V. (2008), Characterization of laser-produced plasma of metal targets. Radiation Effects & Defects in Solids. 163(4-6): 429-433.

[18] Kohno, S., Lisitsyn, I., Kawauchi, T., Katsuki, S., and Akiyama, H. *Characterization of laser-produced plasma in a plasma opening switch*. (1997) 2, 1186-1191: IEEE.

[19] Roshani, G., Habibi, M., and Sohrabi, M. (2011), An improved design of Faraday cup detector to reduce the escape of secondary electrons in plasma focus device by COMSOL. Vacuum. 86(3): 250-253.

[20] Ghadikolaee, M.R.B. and Ghadikolaee, E.T. (2012), Design of a new Faraday cup to measure the beam current of an ion source with residual gas. Journal of fusion energy. 31(6): 569-572.

[21] Naieni, A.K., Bahrami, F., Yasrebi, N., and Rashidian, B. (2009), Design and study of an enhanced Faraday cup detector. Vacuum. 83(8): 1095-1099.

[22] Guethlein, G., Houck, T., McCarrick, J., and Sampayan, S. (2000), Faraday Cup Measurements of Ions Backstreaming into a Electron Beam Impinging on a Plasma Plume*. arXiv preprint physics/0008165.

[23] Giulietti, D. and Gizzi, L.A. (1998), X-ray emission from laser-produced plasmas. La Rivista del Nuovo Cimento. 21(10): 1-93.

[24] Serbanescu, C., Fourmaux, S., Kieffer, J.-C., Kincaid, R., and Krol, A. *K-alpha x-ray source using high energy and high repetition rate laser system for phase contrast imaging*. (2009) San Diego, CA 7451, 745115-745115-9: International Society for Optics and Photonics.

[25] Bukhari, M., Iqbal, S.J., Rafique, M.S., and Iqbal, M. (2013), PRODUCTION OF HARD X-RAY BY LASER PRODUCED PLASMA. Science International-Lahore. 25(4): 687-691.

[26] Flyckt, S.-O., Photomultiplier tubes: principles and applications. 2002: Photonis.

[27] Dey, S., Gupta, D., Maulik, A., Raha, S., Saha, S.K., Syam, D., Pakarinen, J., Voulot, D., and Wenander, F. (2011), Calibration of a solid state nuclear track detector (SSNTD) with high detection threshold to search for rare events in cosmic rays. Astroparticle Physics. 34(11): 805-808.

[28] Bhagwat, A. (1993), Solid State Nuclear Track Detection: Theory and Applications. Published by Indian Society for Radiation Physics, Kalpakkam chapter, ISRP (K)-TD-2.

[29] Bhatti, K., Rafique, M., Khaleeq-ur-Rahman, M., Latif, A., Hussain, K., Hussain, A., Chaudhary, K., Tahir, B., and Qindeel, R. (2011), Characterization of Platinum and Gold ions emitted from laser produced plasmas using solid state nuclear track detectors. Vacuum. 85(10): 915-919.

[30] Iqbal, J., Mahmood, S., Tufail, I., Asghar, H., Ahmed, R., and Baig, M.A. (2015), On the use of laser induced breakdown spectroscopy to characterize the naturally existing crystal in Pakistan and its optical emission spectrum. Spectrochimica Acta Part B: Atomic Spectroscopy. 111: 80-86.

[31] Zhu, X., Xu, T., Lin, Q., Liang, L., Niu, G., Lai, H., Xu, M., Wang, X., Li, H., and Duan, Y. (2014), Advanced statistical analysis of laser-induced breakdown spectroscopy data to discriminate sedimentary rocks based on Czerny–Turner and Echelle spectrometers. Spectrochimica Acta Part B: Atomic Spectroscopy. 93: 8-13.

[32] Dyar, M.D., Tucker, J.M., Humphries, S., Clegg, S.M., Wiens, R.C., and Lane, M.D. (2011), Strategies for Mars remote laser-induced breakdown spectroscopy analysis of sulfur in geological samples. Spectrochimica Acta Part B: Atomic Spectroscopy. 66(1): 39-56.

[33] Gottfried, J.L., Harmon, R.S., De Lucia, F.C., and Miziolek, A.W. (2009), Multivariate analysis of laser-induced breakdown spectroscopy chemical signatures for geomaterial classification. Spectrochimica Acta Part B: Atomic Spectroscopy. 64(10): 1009-1019.

[34] Alvey, D.C., Morton, K., Harmon, R.S., Gottfried, J.L., Remus, J.J., Collins, L.M., and Wise, M.A. (2010), Laser-induced breakdown spectroscopy-based geochemical fin-

gerprinting for the rapid analysis and discrimination of minerals: the example of garnet. Applied Optics. 49(13): C168-C180.

[35] Prochazka, D., Kynický, J., Prochazková, P., Zikmund, T., Novotný, J., Novotný, K., Kizek, R., Petrilak, M., and Kaiser, J. (2014), 3D CHEMICAL MAPPING OF SELECTED GEOLOGICAL SAMPLES USING COMBINATION OF LASER-INDUCED BREAKDOWN SPECTROSCOPY AND uCT.

[36] Ferreira, E.C., Milori, D.M.B.P., Ferreira, E.J., dos Santos, L.M., Martin-Neto, L., and Nogueira, A.R.d.A. (2011), Evaluation of laser induced breakdown spectroscopy for multielemental determination in soils under sewage sludge application. Talanta. 85(1): 435-440.

[37] Díaz, D., Hahn, D.W., and Molina, A. (2012), Evaluation of Laser-Induced Breakdown Spectroscopy (LIBS) as a Measurement Technique for Evaluation of Total Elemental Concentration in Soils. Applied Spectroscopy. 66(1): 99-106.

[38] Ayyalasomayajula, K.K., Yu-Yueh, F., Singh, J.P., McIntyre, D.L., and Jain, J. (2012), Application of laser-induced breakdown spectroscopy for total carbon quantification in soil samples. Applied Optics. 51(7): B149-B154.

[39] Dell'Aglio, M., Gaudiuso, R., Senesi, G.S., De Giacomo, A., Zaccone, C., Miano, T.M., and De Pascale, O. (2011), Monitoring of Cr, Cu, Pb, V and Zn in polluted soils by laser induced breakdown spectroscopy (LIBS). Journal of Environmental Monitoring. 13(5): 1422-1426.

[40] Nicolodelli, G., Marangoni, B.S., Cabral, J.S., Villas-Boas, P.R., Senesi, G.S., dos Santos, C.H., Romano, R.A., Segnini, A., Lucas, Y., Montes, C.R., and Milori, D.M.B.P. (2014), Quantification of total carbon in soil using laser-induced breakdown spectroscopy: a method to correct interference lines. Applied Optics. 53(10): 2170-2176.

[41] Martin, M.Z., Wullschleger, S.D., Garten, C.T., and Palumbo, A.V. (2003), Laser-induced breakdown spectroscopy for the environmental determination of total carbon and nitrogen in soils. Applied Optics. 42(12): 2072-2077.

[42] Martin, M.Z., Wullschleger, S., and Garten, C. *Laser-induced breakdown spectroscopy for environmental monitoring of soil carbon and nitrogen*. (2002) 4576, 188-195.

[43] Martin, M.Z., Mayes, M.A., Heal, K.R., Brice, D.J., and Wullschleger, S.D. (2013), Investigation of laser-induced breakdown spectroscopy and multivariate analysis for differentiating inorganic and organic C in a variety of soils. Spectrochimica Acta Part B: Atomic Spectroscopy. 87: 100-107.

[44] Nguyen, H.-M., Moon, S.-J., and Choi, J. (2015), Improving the application of laser-induced breakdown spectroscopy for the determination of total carbon in soils. Environmental Monitoring and Assessment. 187(2): 1-11.

[45] Flora, G., Gupta, D., and Tiwari, A. (2012), Toxicity of lead: A review with recent updates. Interdisciplinary toxicology. 5(2): 47-58.

[46] Järvinen, S.T., Saarela, J., and Toivonen, J. (2013), Detection of zinc and lead in water using evaporative preconcentration and single-particle laser-induced breakdown spectroscopy. Spectrochimica Acta Part B: Atomic Spectroscopy. 86: 55-59.

[47] Unnikrishnan, V., Nayak, R., Aithal, K., Kartha, V., Santhosh, C., Gupta, G., and Suri, B. (2013), Analysis of trace elements in complex matrices (soil) by Laser Induced Breakdown Spectroscopy (LIBS). Analytical Methods. 5(5): 1294-1300.

[48] Ferreira, E.C., Gomes Neto, J.A., Milori, D.M.B.P., Ferreira, E.J., and Anzano, J.M. (2015), Laser-induced breakdown spectroscopy: Extending its application to soil pH measurements. Spectrochimica Acta Part B: Atomic Spectroscopy. 110: 96-99.

[49] Haider, Z., Munajat, Y.B., Kamarulzaman, R., and Shahami, N. (2015), Comparison of Single Pulse and Double Simultaneous Pulse Laser Induced Breakdown Spectroscopy. Analytical Letters. 48(2): 308-317.

[50] Barefield, J.E., Judge, E., Clegg, S.M., Berg, J., Colgan, J.P., Kilcrease, D.P., Johns, H.M., Le, L.A., Lopez, L.N., and Trujillo, L.A., Laser-Induced Breakdown Spectroscopy (LIBS): Applications to Analysis Problems from Nuclear Material to Plant Nutrients for Sustainable Agriculture, (2014). Los Alamos National Laboratory (LANL).

[51] Sankaran, S., Ehsani, R., and Morgan, K.T. (2015), Detection of Anomalies in Citrus Leaves Using Laser-Induced Breakdown Spectroscopy (LIBS). Applied Spectroscopy. 69(8): 913-919.

[52] Arantes de Carvalho, G.G., Moros, J., Santos Jr, D., Krug, F.J., and Laserna, J.J. (2015), Direct determination of the nutrient profile in plant materials by femtosecond laser-induced breakdown spectroscopy. Analytica Chimica Acta. 876: 26-38.

[53] Kim, G., Kwak, J., Choi, J., and Park, K. (2012), Detection of nutrient elements and contamination by pesticides in spinach and rice samples using laser-induced breakdown spectroscopy (LIBS). Journal of agricultural and food chemistry. 60(3): 718-724.

[54] Li, W., Huang, L., Yao, M., Liu, M., and Chen, T. (2014), Investigation of Pb in Gannan Navel Orange with Contaminant in Controlled Conditions by Laser-Induced Breakdown Spectroscopy. Journal of Applied Spectroscopy. 81(5): 850-854.

[55] Yao, M., Huang, L., Zheng, J., Fan, S., and Liu, M. (2013), Assessment of feasibility in determining of Cr in gannan navel orange treated in controlled conditions by Laser Induced Breakdown Spectroscopy. Optics & Laser Technology. 52: 70-74.

[56] Vítková, G., Novotný, K., Prokeš, L., Hrdlička, A., Kaiser, J., Novotný, J., Malina, R., and Prochazka, D. (2012), Fast identification of biominerals by means of stand-off laser-induced breakdown spectroscopy using linear discriminant analysis and artificial neural networks. Spectrochimica Acta Part B: Atomic Spectroscopy. 73: 1-6.

[57] Vítková, G., Prokeš, L., Novotný, K., Pořízka, P., Novotný, J., Všianský, D., Čelko, L., and Kaiser, J. (2014), Comparative study on fast classification of brick samples by combination of principal component analysis and linear discriminant analysis using

stand-off and table-top laser-induced breakdown spectroscopy. Spectrochimica Acta Part B: Atomic Spectroscopy. 101: 191-199.

[58] Fang, X. and Ahmad, S.R. (2014), Elemental analysis in environmental land samples by stand-off laser-induced breakdown spectroscopy. Applied Physics B. 115(4): 497-503.

[59] Fortes, F., Guirado, S., Metzinger, A., and Laserna, J. (2015), A study of underwater stand-off laser-induced breakdown spectroscopy for chemical analysis of objects in the deep ocean. Journal of Analytical Atomic Spectrometry. 30(5): 1050-1056.

[60] Guirado, S., Fortes, F.J., and Laserna, J.J. (2015), Elemental analysis of materials in an underwater archeological shipwreck using a novel remote laser-induced breakdown spectroscopy system. Talanta. 137: 182-188.

[61] Gong, Y., Choi, D., Han, B.-Y., Yoo, J., Han, S.-H., and Lee, Y. (2014), Remote quantitative analysis of cerium through a shielding window by stand-off laser-induced breakdown spectroscopy. Journal of Nuclear Materials. 453(1–3): 8-15.

[62] Sturm, V., Fleige, R.d., de Kanter, M., Leitner, R., Pilz, K., Fischer, D., Hubmer, G., and Noll, R. (2014), Laser-induced breakdown spectroscopy for 24/7 automatic liquid slag analysis at a steel works. Analytical chemistry. 86(19): 9687-9692.

[63] Wiens, R., Clegg, S., Barefield, J., and Maurice, S. *The Chemcam LIBS and Imaging Instrument Suite on the Curiosity Mars Rover, and Terrestrial Field Testing of LIBS*. (2014) 1, 3737.

[64] Gasda, P.J., Acosta-Maeda, T.E., Lucey, P.G., Misra, A.K., Sharma, S.K., and Taylor, G.J. (2015), Next Generation Laser-Based Standoff Spectroscopy Techniques for Mars Exploration. Applied Spectroscopy. 69(2): 173-192.

[65] Bogaerts, A. and Chen, Z. (2005), Effect of laser parameters on laser ablation and laser-induced plasma formation: A numerical modeling investigation. Spectrochimica Acta Part B: Atomic Spectroscopy. 60(9–10): 1280-1307.

[66] Albert, O., Roger, S., Glinec, Y., Loulergue, J.C., Etchepare, J., Boulmer-Leborgne, C., Perrière, J., and Millon, E. (2003), Time-resolved spectroscopy measurements of a titanium plasma induced by nanosecond and femtosecond lasers. Applied Physics A. 76(3): 319-323.

[67] Sekiguchi, K., Tanaka, K., Moriya, K., and Uchiki, H. (2006), Epitaxial growth of Cu2ZnSnS4 thin films by pulsed laser deposition. Physica Status Solidi (C) Current Topics in Solid State Physics. 3(8): 2618-2621.

[68] Moriya, K., Tanaka, K., and Uchiki, H. (2007), Fabrication of Cu2ZnSnS4 thin-film solar cell prepared by pulsed laser deposition. Japanese Journal of Applied Physics, Part 1: Regular Papers and Short Notes and Review Papers. 46(9 A): 5780-5781.

[69] Palonen, H., Huhtinen, H., and Paturi, P. (2015), Growth Condition Dependence of Microcracks in YBCO Thin Films Pulsed Laser Deposited on <inline-formula> <img

src="/images/tex/24016.gif" alt="\hbox {NdGaO}_{3}"> </inline-formula> (001) Substrates. Applied Superconductivity, IEEE Transactions on. 25(3): 1-4.

[70] Oshima, T., Yokoyama, K., Niwa, M., and Ohtomo, A. (2015), Pulsed-laser deposition of superconducting LiTi2O4 ultrathin films. Journal of Crystal Growth. 419: 153-157.

[71] Sharma, Y., Misra, P., Katiyar, R.K., and Katiyar, R.S. (2014), Photovoltaic effect and enhanced magnetization in 0.9 (BiFeO3)–0.1 (YCrO3) composite thin film fabricated using sequential pulsed laser deposition. Journal of Physics D: Applied Physics. 47(42): 425303.

[72] Chowdhury, M., Kumar Kunti, A., Kumar Sharma, S., Gupta, M., and Janay Chaudhary, R. (2014), Synthesis and characterization of pulsed laser deposited SnO2-Fe2O3 composite thin films for TCO application. The European Physical Journal - Applied Physics. 67(01): null-null.

[73] Lei, L., Liu, X., Yin, Y., Sun, Y., Yu, M., and Shang, J. (2014), Antibacterial Ag–SiO2 composite films synthesized by pulsed laser deposition. Materials Letters. 130: 79-82.

[74] Pradhaban, G., Kaliaraj, G., and Vishwakarma, V. (2014), Antibacterial effects of silver–zirconia composite coatings using pulsed laser deposition onto 316L SS for bio implants. Progress in Biomaterials. 3(2-4): 123-130.

[75] Eraković, S., Janković, A., Ristoscu, C., Duta, L., Serban, N., Visan, A., Mihailescu, I.N., Stan, G.E., Socol, M., Iordache, O., Dumitrescu, I., Luculescu, C.R., Janaćković, D., and Miškovic-Stanković, V. (2014), Antifungal activity of Ag:hydroxyapatite thin films synthesized by pulsed laser deposition on Ti and Ti modified by TiO2 nanotubes substrates. Applied Surface Science. 293: 37-45.

IntechOpen